Electrical Impedance Spectroscopy for Real-Time Monitoring of the Life Cycle of Graphene Nanoplatelets Filters for Some Organic Industrial Pollutants

Gianfranco Miele, *Senior Member, IEEE*, Stefano Bellucci, Antonino Cataldo, Alessio Di Tinno, Luigi Ferrigno, *Senior Member, IEEE*, Antonio Maffucci, *Senior Member, IEEE*, Laura Micheli, and Sarah Sibilia

***Abstract*— This article proposes an approach for smart monitoring of the life cycle of innovative graphene-based filters for water remediation in the presence of pollutants. The measurement technique is based on suitable figures of merit that analyze the time variation of the electrical impedance frequency spectrum. The proposed study considers the remediation of two toxic industrial pollutants, such as the acetonitrile and the 2,4-dichlorophenol. The contribution of this article is twofold. The first is the demonstration of a reliable monitoring setup that is able, for the selected use cases, to correlate in real time the behavior of the electrical impedance of the filter to its status, defined as "absence of pollutants" and/or "saturation." The second contribution is the proposal of suitable figures of merit, based on measurement of the impedance frequency spectrum, able to increase the measurement sensitivity and the reliability and to mitigate some sources of uncertainty typically associated with these kinds of setups and measurements. Results show that the proposed graphene-based filters combine very good filtering capability and high sensitivity of the electrical impedance to the considered pollutants. These results suggest further investigations with other pollutants and the potential use of this technique for the predictive maintenance of the water filters in industrial applications, by endowing the graphene filters of smart sensing devices.**

***Index Terms*— Electrical impedance spectroscopy (EIS), environmental remediation, graphene nanoplatelets (GNPs), multifrequency analysis, pollution filters, real-time measurement systems.**

Manuscript received February 22, 2021; revised May 19, 2021; accepted May 26, 2021. Date of publication June 14, 2021; date of current version June 30, 2021. This work was supported in part by the Italian Ministry of University and Research through the Smart Distributed System Project (program "Dipartimenti di Eccellenza 2018–2022"), in part by the Project "2D material-based low cost SENSor of aggressive substancEs (2DSENSE)," funded by NATO under the SPS Programme, grant #G5777, and in part by the Italian Ministry of University and Research through the Project "C4E—Monitoraggio degli sversamenti illegali attraverso l'impiego sinergico di tecnologie avanzate" under Grant ARS01_00927. The Associate Editor coordinating the review process was Dr. He Wen. *(Corresponding author: Gianfranco Miele.)*

Gianfranco Miele, Alessio Di Tinno, Luigi Ferrigno, Antonio Maffucci, and Sarah Sibilia are with the Department of Electrical and Information Engineering, University of Cassino and Southern Lazio, 03043 Cassino, Italy (e-mail: gianfranco.miele@unicas.it; alessio.ditinno@unicas.it; luigi.ferrigno@unicas.it; antonio.maffucci@unicas.it; sarah.sibilia@unicas.it).

Stefano Bellucci is with the Istituto Nazionale di Fisica Nucleare–Laboratori Nazionali di Frascati (INFN-LNF), National Institute of Nuclear Physics, Frascati National Laboratories, 00044 Frascati, Italy (e-mail: stefano.bellucci@lnf.infn.it).

Antonino Cataldo is with the Department of Information Engineering, Polytechnic University of Marche, 60121 Ancona, Italy, and also with the Istituto Nazionale di Fisica Nucleare–Laboratori Nazionali di Frascati (INFN-LNF), National Institute of Nuclear Physics, Frascati National Laboratories, 00044 Frascati, Italy (e-mail: antonino.cataldo@lnf.infn.it).

Laura Micheli is with the Department of Chemical Science and Technologies, University of Rome "Tor Vergata," 00133 Rome, Italy (e-mail: laura.micheli@uniroma2.it).

Digital Object Identifier 10.1109/TIM.2021.3089247

I. Introduction

THE current industrial era, namely the Industry 4.0, is subjecting modern manufacturing companies to new environmental, technological, and managerial challenges [1]–[3]. In this scenario, companies are trying to reduce their impact on the environment, by increasing efficiency and reducing waste and maintenance costs [2], [3]. The development of technologies that enable the predictive maintenance of pollution filters for water remediation is an example of a new issue of this modern industrial era. These filters must be kept efficient and reliable, to ensure the needed level of health and safety. Their maintenance represents a significant management cost within the production process. This cost is likely to be so high that it could be preferred to replace the filters even if they may still have a working life. For all these reasons, new techniques and methods are proposing in the literature, to enable predictive maintenance, through the real-time monitoring of the filters' life cycle (LC).

The filtering technologies so far assessed, such as the activated carbon filters (ACFs), have been demonstrated to be reliable and effective in removing or reducing a large variety of contaminants from air and water [4]. This technology was also proved to be suitable for effective real-time monitoring during the use, as recently shown in [5]. However, ACFs present three weak points: 1) a limited range of adsorbed pollutants (e.g., they do not show good efficiency in removing metals, bacteria, or viruses); 2) a nonnegligible environmental impact of the fabrication process; and 3) the impossibility of a complete filter regeneration after the use.

These and other unsolved issues related to the use of ACFs are suggesting in recent years to investigate novel materials, such as graphene and graphene-based nanomaterials. Due to its outstanding properties [4], graphene has been proposed for the realization of new filters for pollution remediation [6], [7]. These filters have shown excellent adsorbing capacities also

toward dyes, antibiotics, and heavy metals [8]–[12] and present very good performance if compared to the ACFs [5], [13].

Different graphene-based filters have been so far realized, by using synthetic graphene oxide [8], [9], functionalized structures such as metallic nanomaterials grown on graphene sheets [7], carbon nanotubes [11], and hybrid carbon nanotube-graphene arrangements [12]. After having demonstrated their effectiveness, the research community is now focusing on the assessment of a suitable fabrication process with the final aim of scaling up the production of graphene filters to high rates and low sale costs while guaranteeing the requested levels of reproducibility and reliability: this is, however, still an open challenge.

Trying to overcome these limitations, recently, the efforts have been focused on graphene-related low-cost materials, such as the so-called graphene nanoplatelets (GNPs). Indeed, this material is expected to combine large-scale production and low costs with remarkable physical properties. From this point of view, many promising fabrication techniques have been developed, such as those based on liquid-phase exfoliation procedure, ball milling [14], and the microwave radiation of intercalated graphite. The latter technique has been recently assessed by the authors and has been used to produce the pollutant filters adopted in this article [15], [16]. In addition, we have successfully presented a methodology based on the electrical impedance spectroscopy (EIS), for the real-time monitoring of the state of health (SoH) of both ACF filters [5], [17] and GNP ones [18].

In this article, starting from their experience in real-time impedance measurements [19]–[21], we propose a significant advancement on the abovementioned EIS methodology, presenting a measurement approach based on the definition of suitable figures of merit that analyze the time variation of the electrical impedance frequency spectrum. Indeed, although the single-frequency method proposed in [18] highlights some benefits and theoretically allows revealing some states of the monitored filters, in many cases, the uncertainties related to the filter reproducibility, the measurement repeatability, the setup nonidealities, the interactions between the filter and the pollutant, and the aging of the filter might reduce the state detection capability. Therefore, starting from the preliminary encouraging results presented in [22], this article proposes the analysis of the electrical impedances at different frequencies to increase the capability to detect the operating state of the filter. In detail, this approach allows a measurement method that removes the need of absolute references, which can be strongly influenced by the above-described nonidealities. For a better generalization of the proposed methodology, two different classes of pollutants, with complementary physical and chemical properties, have been considered.

This article is organized as follows. In Section II, the graphene filter, the pollutants, and their interaction are described. Section III reports the designed measurement setup along with the impedance model. Results are presented and discussed in Section IV. Conclusion follows in Section V.

II. Graphene Filter and the Selected Pollutants

The pollution filters realized for the present work have been fabricated by pressing a powder of GNP flakes obtained with the technique described in [15] and [16]. Specifically, the GNPs have been obtained with microwave irradiation, sonication, and final vacuum filtration processes applied to low-cost intercalated graphite distributed by Asbury Carbons Inc. These processes allow controlling the GNP lateral size and obtaining graphene materials with less than ten layers. Low thickness values are essential in retaining outstanding physical properties such as those of 2-D materials that are at the basis of the excellent adsorption performance of the graphene filters. In addition, this fabrication technique provides high-quality samples, with negligible oxidation and a good level of purity of the material, as demonstrated by the Raman and X-ray characterization carried out in [18].

TABLE I
Experimental Data for Adsorption Factor (Acetonitrile) and Density of Filter at Different Loads

Load [N]	Adsorption factor (AF) [%]	Standard deviation of the adsorption factor (σ_{AF}) [%]	Density (ρ) [kg·m^3]
425	169.9	0.17	257
700	139.6	0.20	398
3000	40.5	4.2	785

The fabricated GNP flakes have been then pressed to form thin disks. As shown in Table I, the capability of pollutant adsorption decreases when the load due to the reduction of porosity increases. Although the best adsorption occurs at low load, the filter has low density [16] and this causes a fragile behavior that produces handling deformation. From these considerations, a pressure of 700 N was chosen, as the value that provides an optimal tradeoff between mechanical robustness and adsorption capacity [16].

Several samples of the filters have then been produced with the diameter ranging from 2.8 to 3.2 cm, the thickness between 0.6 and 0.7 mm, and the weight between 0.18 and 0.21 g. Microscopic details of the surface of one of the realized filters are reported in Fig. 1 that also shows the situation before and after the pressing of the disks, to highlight the flakes alignment due to the pressing procedure. In this article, the GNP filters have been used to adsorb two industrial pollutants: 1) acetonitrile (CH_3CN) and 2) 2,4-dichlorophenol ($Cl_2C_6H_4O$).

The acetonitrile is the simplest organic nitrile (any organic compound that has a $-C \equiv N$ functional group), mainly found as a by-product of acrylonitrile manufacture in pharmaceuticals, perfumes, rubber products, photographic film, pesticides, and batteries. People may be exposed to this compound by breathing in the chemical, by drinking contaminated water from a facility where it is stored or used or by eating food that has been previously contaminated with acetonitrile [23], [24].

The 2,4-dichlorophenol is a white, mildly acidic (pKa $=$ 7.9) solid, belonging to chlorophenols. These toxic chemical compounds constitute a serious threat to environmental health due to their harmful effect and persistence in natural matrices. These semivolatile organochloride compounds are easily detected in surface and ground waters, tap and industrial wastewater, atmosphere air, and soils [25].

In this article, the choice of these two pollutants, related to industrial production, was suggested by the need to investigate the response of the filters to contaminants with different and

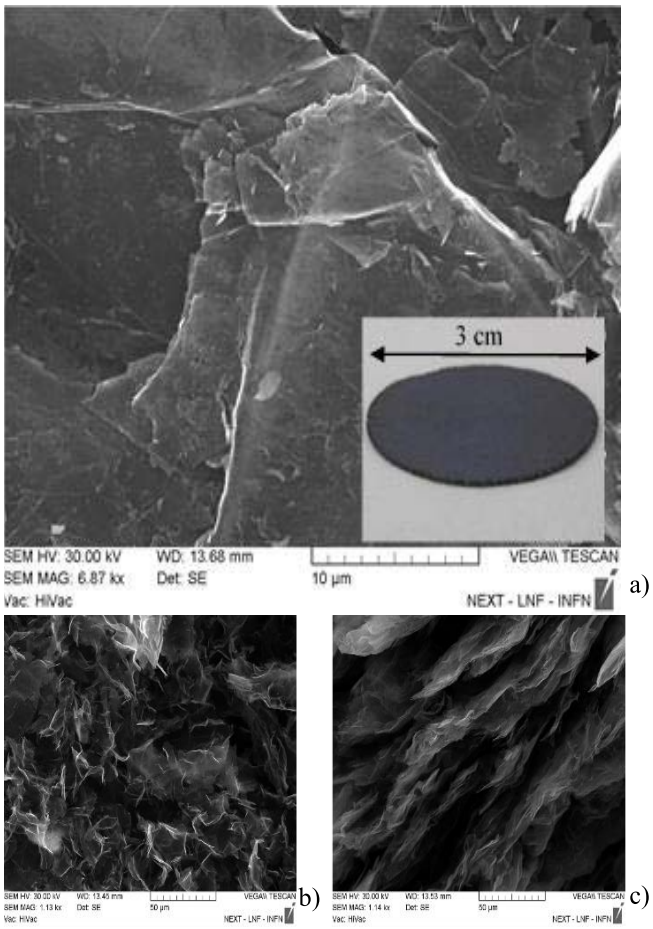

Fig. 1. Scanning electron microscopic image of the surface of the GNP filter. (a) Surface arrangement of the flaks. Inset: pressed GNP filter. (b) Surface before the 700-N press procedure (photo resolution of 50 μm). (c) Surface after the 700-N press procedure (photo resolution of 50 μm).

complementary characteristics. In this way, a comprehensive spectrum of working operating conditions could be covered, allowing the possible generalization of the analysis results. More specifically, it results that the following conditions hold: 1) the acetonitrile is completely soluble in water, whereas the 2,4-dichlorophenol is not soluble; 2) the acetonitrile tends to evaporate spontaneously, whereas the 2,4-dichlorophenol does not evaporate and persists in the filter; and 3) the two pollutants have different interactions with the GNP-based filters. As for the last point, as observed in [26], molecules with higher molecular weights (such as 2,4-dichlorophenols ones) are easily adsorbed onto the outer surface of the nanomaterial, while smaller molecules (such as acetonitrile ones) are entrapped inside the micropores [27]. In addition, the presence of aromatic rings (2,4-dichlorophenols) also guides the removal of organic pollutants by carbon-based nanomaterials: aromatic structures can form stabilizing π–π interaction (face to face, edge to face, or parallel-displaced) with carbonaceous nanomaterials, thus facilitating their removal from aqueous environments with respect to aliphatic organic molecules [28].

III. Setup and Measurement Procedure

As highlighted in Section I, the proposed method is based on the monitoring of the time variation of the electrical

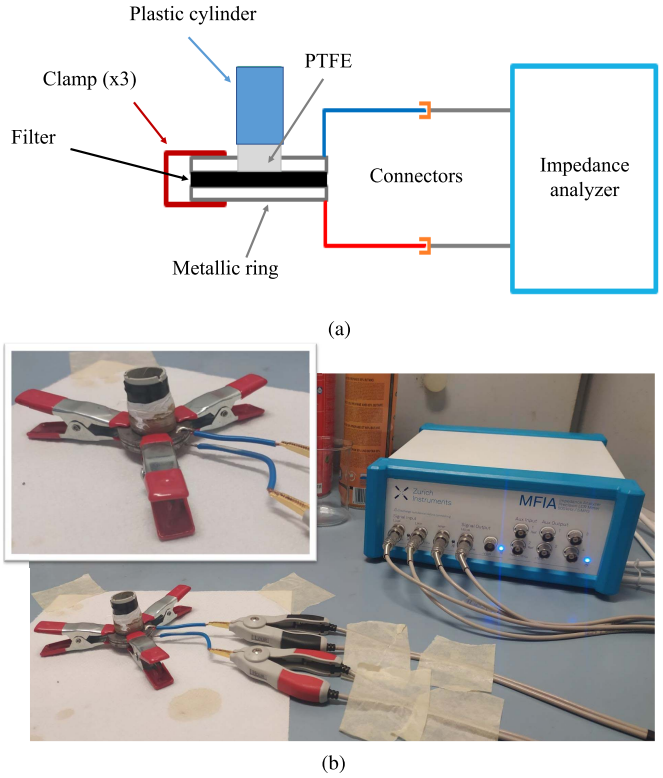

Fig. 2. (a) Schematic and (b) photograph of the electrical setup with details about the test fixture and the connection to the measurement instrument.

impedance frequency spectrum of the filter when exposed to pollutants. These changes happen due to the sensitivity of the graphene electrical properties (e.g., conductivity and permittivity) with the binding of external substances [18], [28]. It is worthy to stress that the sensitivity and selectivity to target substances can be strongly enhanced by a suitable functionalization process [29], [30] so that these materials are currently proposed, for instance, as sensing elements in environmental sensor platforms [31], [32]. The final goal of the proposed research is to detect the presence of the contaminant and to predict the filter lifetime by distinguishing between three conditions: "clean," "adsorption," "saturation."

In this section, details about the realized setup and the developed measurement procedure are given.

A. Realized Measurement Setup

A suitable measurement setup has been realized, to inject known quantities of pollutant, estimate the environmental conditions, highlight the interaction between the filter and the pollutant, and monitor the time evolution of the electrical parameters.

In detail, Fig. 2(a) sketches a scheme of the setup and the connections, while in Fig. 2(b), a photograph of the whole system is reported. Looking at Fig. 2(a), the setup is composed of three main sections: 1) the system to inject the pollutant; 2) the test fixture; and 3) the measurement section. As for the system to inject the pollutant 1), from the top side, a plastic cylindrical tube is placed on the filter, realizing a filter-tube connection like those adopted in an industrial environment. In this tube, the pollutant is injected and dosed in known

and controlled quantities. In addition, a polytetrafluoroethylene (PTFE; also known as Teflon) layer provides the insulation between the metal contacts and the pollutant, ensuring that only the filter is in direct contact with the pollutant [18], [33].

As for the text fixture, Fig. 2 shows the details on the schematic layout and on its realization. It consists of two hollow metal rings that contact the graphene filter and allow the connection to the measurement instrument through two short wires. This connection has been required to avoid the direct contact between the pollutant and the clamp of the measurement instrument. In this way, we avoid that drops of pollutant on the instrument's clamp may affect the measured impedance. These two wires are about 3 cm long. This length is a compromise between the dimensions required to install the system under the extractor hood during the experiments, and the minimum dimensions required to minimize parasitic effects due to the wire. In any case, as described in the following, a suitable calibration procedure can mitigate the effect of these wires. Then, these wires are connected to a four-wire measurement setup to reduce the effect of long cables in the measurement procedure (see Fig. 3). The measurement instrument has been programmed to measure the real and imaginary parts of electrical impedance in the frequency range from 1 to 100 kHz. Looking at the parasitic effects, a simple circuit model can be adopted for the setup (see Fig. 3), where the filter is represented by a series impedance $Z_S = R_S + iX_S$, whereas all the contributions coming from the setup are included in the parasitic components R_P, L_P, and C_P.

As for the physical meaning of the considered parasitic parameters, some considerations can be made. Indeed, even if the four-probe connection with the measurement instrument allows the compensation of the effect of the cables, the effect of resistive, inductive, and capacitive coupling between the filter contacts and the instrument cables is still present. In detail, the resistive parasitic effects are due to the two short wires in the setup, the resistance of the electrodes, and the contact resistances that appear in the weld contact with the filter and in the contact with the clamps of the measurement instrument. Given the analyzed frequency range, it is possible to assert that typically, these parasitic effects will be very similar for all the considered frequencies. As for the inductive parasitic effects, they are associated with the loop formed by the two wires and the instrument clamps. This loop generates a magnetic field and could sense unwanted magnetic fields. Since the two wires cannot be wounded not to reduce the length, this effect should be mitigated during the calibration procedure. The last parasitic effect is due to unwanted capacitive couplings between the two wires, the two rings, and each wire and ring with the environment. The best way to reduce the weight of the parasitic effects would have been that of providing the specimen with a metallic shield, but this solution cannot be pursued, due to the need of having enough clearance to insert the pollutant in the tube. In these conditions, during each test, to mitigate the parasitic effects, the setup has been placed 2 m away from other electric or electronic devices, in fixed environmental conditions and without modifying the geometry during the test. In addition, for each experiment, a calibration (open/short) procedure has been performed to compensate

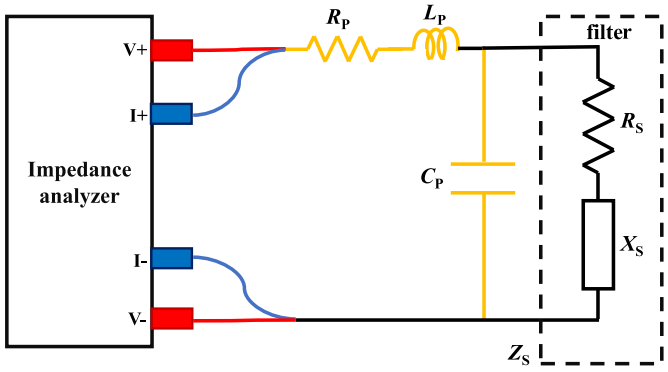

Fig. 3. Equivalent circuit model for the experimental setup in Fig. 2.

TABLE II
VALUES OF THE ELECTRODES IMPEDANCES BEFORE AND AFTER THE CALIBRATION PROCEDURE

	R_S [mΩ]	X_S [mΩ]
Before calibration	22.02	391.7
After calibration	-0.68	-0.05

for the remaining parasitic or unwanted effects. According to the scheme in Fig. 3, the impedance of the electrodes is compensated by the open/short calibration procedure. In the short procedure, the two hollow ring electrodes are clamped together, without the filter, and the short-circuit impedance is estimated for all the considered frequencies. This impedance is then removed by the impedance meter during the measurement process. In Section III-B, further details about the calibration procedure are given to quantify and remove all the considered parasitic effects.

In addition, to have good contacts between the rings and the filter, assure always the same mechanical pressure, and give stability to the parasitic capacitance, three isolated clamps are used to press the rings on the filter. In this way, for each experiment, the resistance due to the nonideal contact is kept at a minimum value and parasitic effects, associated with the geometry, are kept almost of the same order of magnitude.

To evaluate the whole weight of the parasitic effects, Table II reports the values of the whole impedance measured when the hollow ring electrodes are clamped without the filter and at a frequency of 100 kHz before and after the calibration procedure. It can be highlighted that the values obtained after the calibration procedures are residuals if compared with those experienced in the presence of the GNP filter.

As for the measurement instrument 3), the electrical impedance has been here measured by means of a Zurich Instruments MFIA Impedance Analyzer, which allows measuring up to 5 MHz with a basic accuracy of about 0.05% [22]. In addition, two auxiliary instruments, not reported in Fig. 2, have been considered to weigh the filter and to measure the environmental condition of each experiment. To weigh the filters, the Kern ABS 80-4N analytical balance has been adopted. It allows a resolution of 0.1 mg that is suited for the considered applications. Finally, a digital thermometer completes the measurement setup. It controls the environmental condition stability during the measurements. As discussed in Section III-B, this is an important aspect of

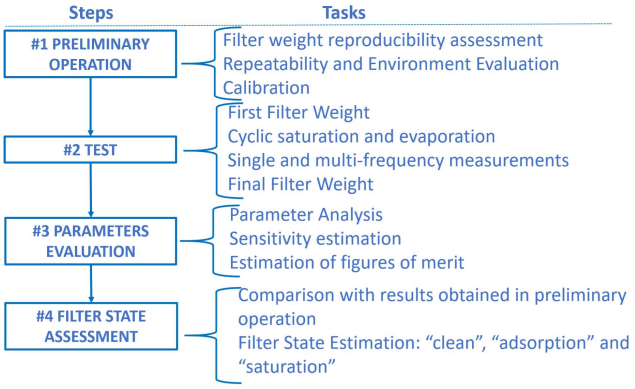

Fig. 4. Proposed measurement procedure.

the measurement procedure since a preliminary analysis has highlighted the variation of the graphene filter's properties with the temperature.

B. Realized Measurement Procedure

As stated above, six GNP filters have been realized for the experimental campaign. The geometrical dimensions of the filters have been chosen to match the measurement setup. As described above, these cylindrical filters have been obtained starting from a reference weight of about 0.2 g of material.

The proposed measurement procedure (see Fig. 4) is composed of four steps, namely: (step #1) the preliminary operation, (step #2) the test, (step #3) the parameter evaluation, and the filter state assessment (step #4). In detail, during step #4, the use of suitable thresholds allows the determination of the filter status: "clean," "adsorption," or "saturation."

In the preliminary step, the six filters have been characterized in terms of weight and dimensions. In detail, they show a mean weight of 0.191 g, with a percentage standard deviation of 5.7%, a mean diameter equal to 30.3 mm, with a percentage standard deviation of 5.7%, and a mean thickness of 0.63 mm, with a percentage standard deviation of 8.1%. These values confirm the good reproducibility in the production of filters. Then, looking at the scheme of Fig. 4, the standard deviations of the considered electrical parameters have been evaluated in the absence of pollutants, both at a reference temperature (i.e., 21 °C) and different environmental temperatures. At the reference temperature, the experimented standard deviation in the absence of pollutant is always better than 0.04% (for R_S) and 0.8% (for X_S). Changing the environmental temperature from 21 °C to 45 °C, the considered standard deviations worsen, with a further stability coefficient equal to 4% for both the R_S and X_S parameters. Since this deviation might hide the presence of the pollutant in some measurement results, the room temperature has been controlled during each experiment and kept at the fixed value of 21 °C ± 2 °C, as it happens in calibration laboratories for electrical quantities.

After these activities, a proper calibration phase has been executed to mitigate the parasitic effects described in Section III-A, namely R_P, L_P, and C_P in Fig. 3. In detail, the typical open/short compensation stages have been performed. In this calibration, we have chosen to consider also the metal rings during the open/short procedure. In detail, during the short calibrations, the two rings have been placed in contact, pressed with the three clamps described above. In this way, the overall resistance and the stray inductance have been estimated. In the open calibration, the two rings have been placed at the same distance that can be found when the graphene-based filter is inserted, but without the filter. Two little plastic spacers accomplish this task allowing the rings to be separated by air. This calibration phase allows evaluating and compensating the overall parasitic capacitance. Given the considered circuit and all the setup limitations described above, this calibration procedure has been executed before each test, to compensate for the effects of all the external components R_P, L_P, and C_P of the parasitic impedance that might vary during the time.

Before the execution of the measurement activities, a preliminary analysis aimed at assessing the sensitivity, the repeatability, the filter reproducibility, the frequency, and the thermal stability has been carried out, following the example of what done in [18] and [33]. For the sake of brevity, its results are not reported in this article.

After this preliminary phase, several tests have been executed (step #2). As shown in Fig. 4, before each test, the considered filter has been weighted to verify its "clean" state. The same weighing procedure has been performed at the end of each test. Indeed, when the test considers a saturation of the filter, measuring that the weight is the way to estimate the quantity of pollutant that the filter has been able to retain. Instead, when the test considers a saturation–evaporation phenomenon, since it is not possible to weigh the filter at the end of the saturation stage without stopping the experiment and recalibrating the measurement setup, the weight is performed at the end of the evaporation phase and is used to confirm the new clean state of the filter. Specifically, in the case of the (volatile) acetonitrile, the filter final weight can certify its evaporation at the end of the observation period. As for the nonvolatile 2,4-dichlorophenol, the weighting procedure can certify the quantity of pollutant that the filter has been able to retain at the end of the experiment.

In each experiment, for each considered pollutant and during each experiment, a controlled quantity (of the order of some milliliters) of pollutant was manually dropped into the hollow cylinder by using an automatic pipette in a controlled time.

Finally, steps #3 and #4 are executed after each test. Details on these two steps are given in the following.

IV. Results and Discussion

Considering the different characteristics of the two pollutants (i.e. the first is volatile and the second not) and their different interactions with the filter, four different experiments have been carried out, aiming at emulating possible real-case operating conditions.

The first two experiments involved the acetonitrile. In the first one (test #1), a quantity of pollutant has been injected up to the filter saturation and the time evolution of the filter electrical impedance has been monitored until the complete evaporation. In the second test (test #2), this cycle has been repeated twice, to simulate a repetitive industrial process and to have a confirmation about the behavior of the filter.

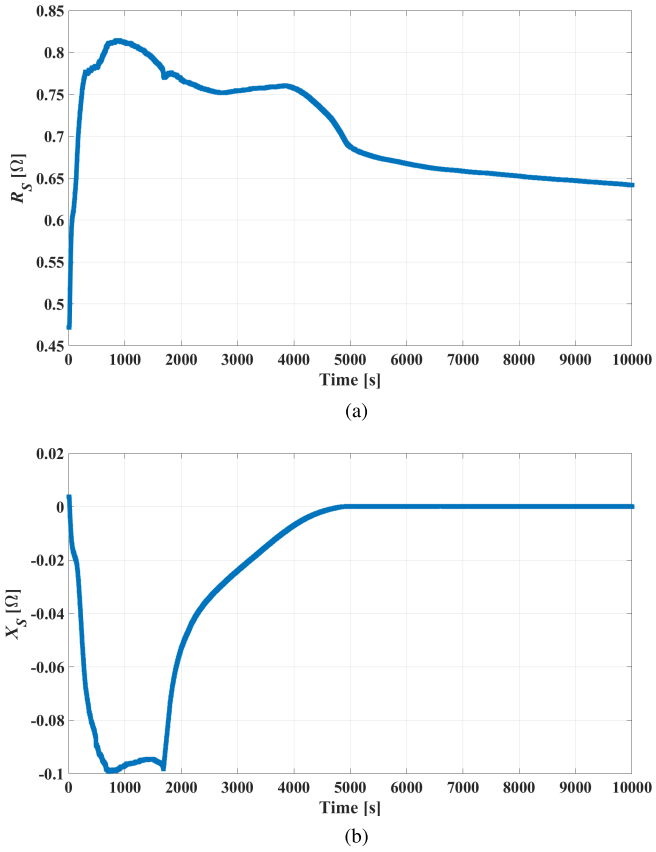

Fig. 5. Time behavior of (a) figures of merit R_S and (b) X_S for test #1 (acetonitrile, single excitation frequency of 100 kHz).

In the other two experiments, the 2,4-dichlorophenol has been considered. In the third one (test #3), a small quantity has been injected (0.1 mL), lower than the minimum quantity (0.5 mL) necessary to saturate the filter. This injection has been repeated six times at controlled time instants. This test allows verifying a slow filter–pollutant interaction, also to highlight the proposed setup sensitivity. For evaluating the promptness of the filter, a fourth experiment (test #4) has been designed, in which a quantity of pollutant equal to 0.5 mL was injected in a single step. In all cases, the filter has been monitored for a time interval sufficient to consider expired all the transients.

In the following, the results obtained in [18] and [33] by a single-frequency EIS are presented and discussed. Then, in Section IV-B, the results obtained with the proposed multifrequency approach are presented and compared to those obtained at a single frequency.

A. Single-frequency Analysis

In the experiments carried out in [18], [22], and [33], a single excitation frequency equal to 100 kHz was considered. In Fig. 5, the results of test #1 (acetonitrile) are reported, in terms of the time behavior of the real and imaginary parts of the impedance, R_S and X_S. As previously described, in test #1, the pollutant was injected in a quantity greater than the filter retaining capability, to be sure to lead the filter to saturation. The time evolution of the electrical parameters in Fig. 5 highlights some special states of the filters. In detail, when the pollutant is injected, R_S increases [Fig. 5(a)], while X_S decreases [Fig. 5(b)], becoming negative, thus moving from an inductive to a capacitive behavior.

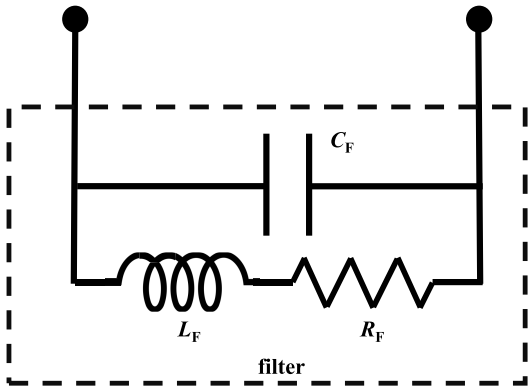

Fig. 6. Simple equivalent model of the filter impedance.

A simple equivalent model of the filter impedance Z_S is reported in Fig. 6. It may be given by the parallel of a capacitor and of a resistor (the latter may also be augmented with a series parasitic inductor).

Considering that the instrument models the impedance as $Z_S = R_S + iX_S$ (see Fig. 3), the following relations hold with respect to the model reported in Fig. 6:

$$R_S = \frac{R_F}{1+\omega^2 C_F^2\left(R_F^2+\omega^2 L_F^2-2\frac{L_F}{C_F}\right)} \tag{1}$$

$$X_S = \frac{\omega L_F(1-R_F^2\frac{C_F}{L_F}-\omega^2 L_F C_F)}{1+\omega^2 C_F^2\left(R_F^2+\omega^2 L_F^2-2\frac{L_F}{C_F}\right)}. \tag{2}$$

The capacitive behavior is associated with the equivalent dielectric constant of the filter, ϵ_r, whereas the resistive behavior is obviously related to the filter equivalent conductivity, σ. As the pollutant is adsorbed, the deformation of the lattice and the presence of external elements lead to the decrease of the conductivity σ and the increase of the relative electrical permittivity ϵ_r, whereas the relative magnetic permeability μ_r is almost insensitive, since the pollutant has no magnetic property. This is coherent with the results in Fig. 5. During the adsorption, the increase of ϵ_r leads to an increasing $|X_S|$, whereas the opposite behavior is found during the evaporation of the pollutant [see Fig. 5(b)]. After the complete cycle adsorption–saturation–evaporation, the dielectric constant ϵ_r (and hence the reactance, X_S) comes back to the initial value. The observed behavior of the resistance R_S [Fig. 5(a)] is more complicated, with a phase of increase (during the adsorption), coherent with the expected behavior of σ, but with a subsequent phase of nonmonotonic decrease. The final value significantly differs from the initial one. The behavior of R_S is probably related to an aging effect of the pollutant with the ring contacts and/or to the liquid–gas phase transition of the acetonitrile before its evaporation, which may have changed locally the pressure, resulting in an increased distance between the GNPs.

In any case, this behavior may limit the applicability of detection algorithms that are based on thresholds. Looking at the X_S parameter, even though in this test it shows the

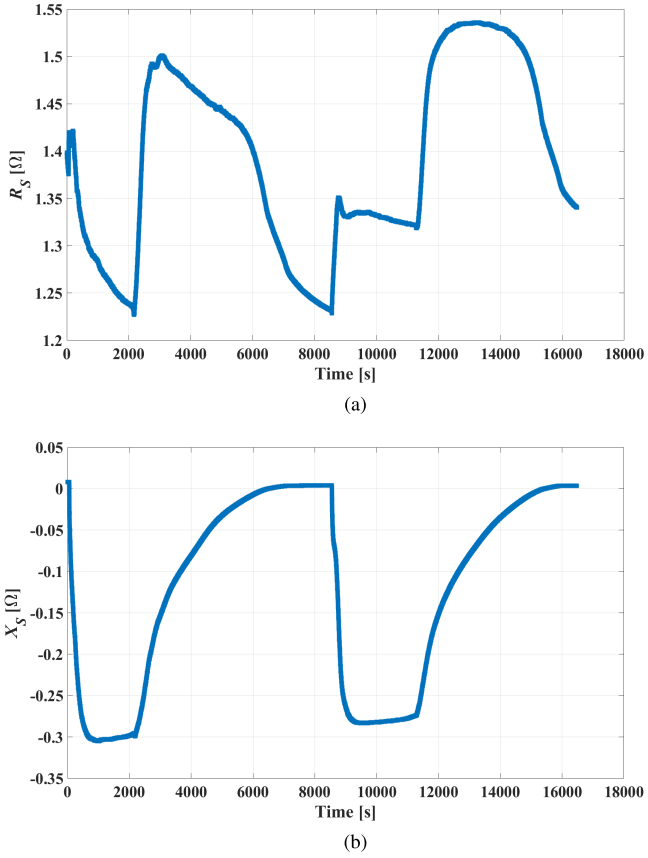

Fig. 7. Time behavior of figures of merit: (a) R_S and (b) X_S for test #2 (double cycle of acetonitrile, single excitation frequency of 100 kHz).

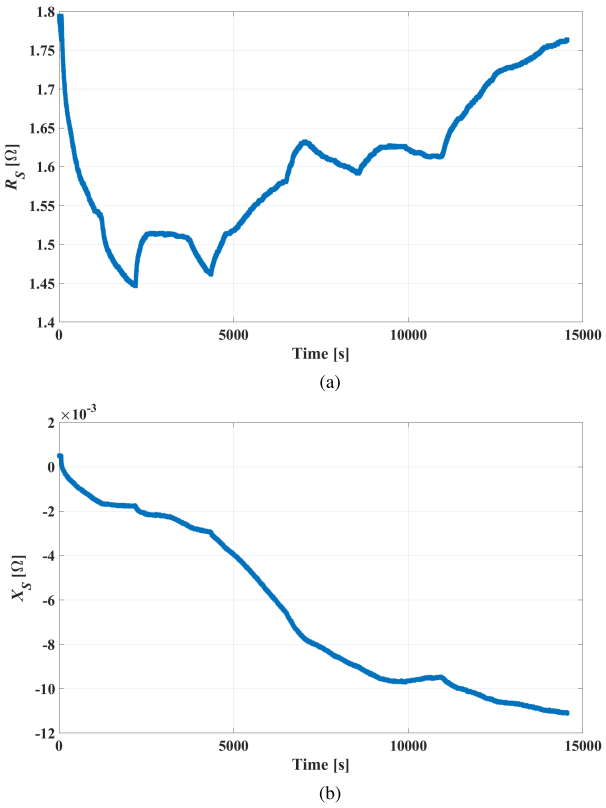

Fig. 8. Time behavior of figures of merit: (a) R_S and (b) X_S for test #3 (2,4-dichlorophenol, single excitation frequency of 100 kHz).

theoretically expected behavior, with a starting value equal to 0 Ω and being negative in the presence of pollutant, it has to be noticed that sometimes, due to calibration or parasitic effects, the starting value could significantly differ from zero in the absence of pollutant. This phenomenon might limit the application of a threshold-based method that observes the sign of X_S.

Fig. 7 reports the results related to the second experiment involving acetonitrile (test #2), where a double cycle has been simulated; after the first cycle, the second injection has been performed after waiting for a time interval sufficiently large for the filter to clean again, under the action of the evaporation of the acetonitrile. In this way, we have simulated two consecutive filtering cycles. These results clearly highlight all the filter stages as in the first case; after the acetonitrile was completely evaporated, the filter started again to work with the same performance as in the first cycle. However, similar issues to those noticed in test #1 are present also in this case.

In Fig. 8, the experimental results of test #3 involving the 2,4-dichlorophenol pollutant are reported. As described above, in this test, the saturation quantity (0.5 mL) was reached gradually, by five subsequent injections of smaller quantities (0.1 mL) at controlled time instants. The results, reported in Fig. 8, provide an unreliable behavior of the R_S parameter, which does not allow the correct identification of the filter operating stages. This is due to a strong interaction of the pollutant with the ring contacts that directly feel the substance, together with the indirect measurement done through the filter. On the contrary, the X_S parameter shows a reliable result, highlighting the different injection phases. Nevertheless, the same problems of the acetonitrile cases, due to the difference in the starting value of X_S, are also experimented for this pollutant.

Finally, Fig. 9 reports the results of test #4, in which, after a preliminary stage with the filter operating without the presence of any pollutant, a quantity of 0.5 mL of 2,4-dichlorophenol has been injected in a single step, able to saturate the filter.

Besides the limits already pointed out, these results put on evidence that the monitored electrical parameters exhibit a completely different behavior, which does not allow to correctly identify the filter operating stages. This problem can be solved by moving from a single to a multifrequency approach.

B. Multifrequency Analysis

This approach introduces a relative measurement paradigm that removes the need of monitoring the absolute references, strongly influenced by the interaction with the contacts with the pollutant, the aging of the filter, the change in the environmental parameters, and so on. In detail, knowing that pollutants are differently influenced by different excitation stimuli, we aim at using the behavior at given frequencies as a reference and at estimating the filter SoH by referring to such a reference behavior. To this aim, two experimental multifrequency measurement campaigns have been carried out, for each of the two considered pollutants, by using seven frequency values to excite the filter, ranging from 1 to 100 kHz.

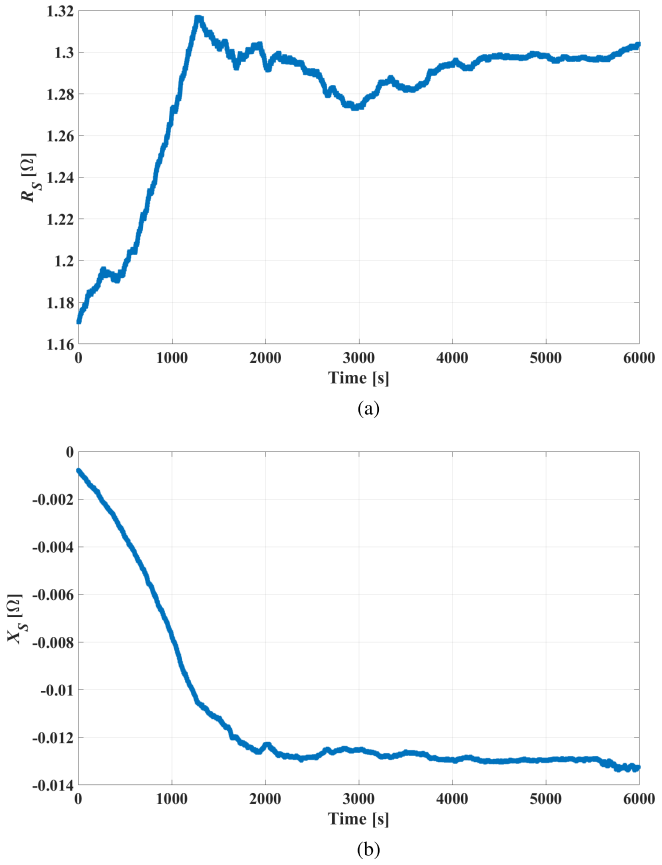

Fig. 9. Time behavior of figures of merit: (a) R_S and (b) X_S for test #4 (2,4-dichlorophenol, single excitation frequency of 100 kHz).

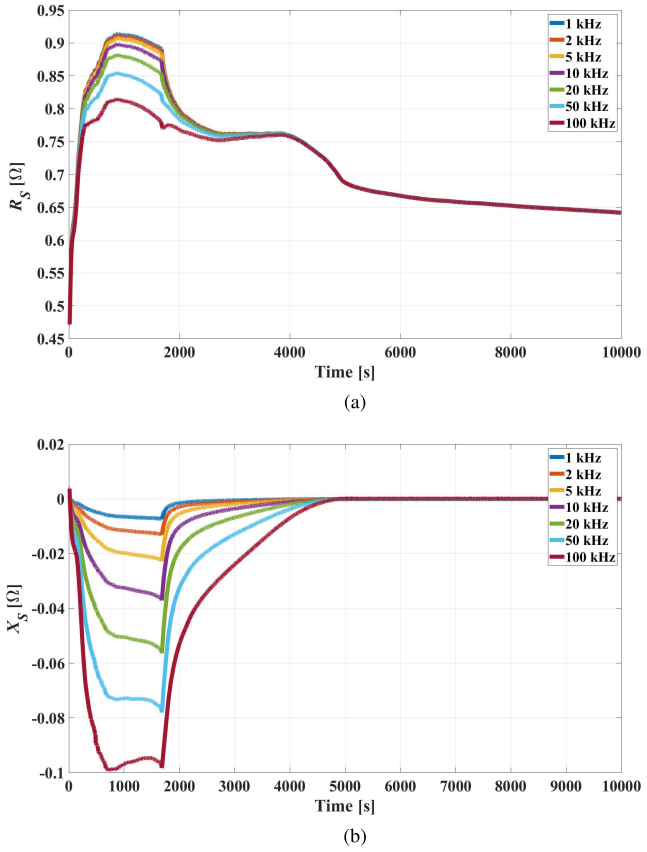

Fig. 10. Time behavior of figures of merit: (a) R_S and (b) X_S for test #1 (acetonitrile, multifrequency analysis, seven frequencies from 1 to 100 kHz).

This is the minimum set of frequencies that allow to cover the considered range with regular spacing in the logarithmic scale. A good covering of this range is important in order to check whether the impedance measurements for all the frequencies follow the same trend or if some anomalies in the frequency behavior are present.

The results of this multifrequency analysis obtained for test #1 (acetonitrile) are reported in Fig. 10, with a very long observation time after the filter has saturated. For all the considered frequencies, it is possible to highlight that the R_S and the X_S parameters show a rapid change in their value. These behaviors are very similar for the two parameters and highlight the presence of the pollutant. A very important result arising from Fig. 10 is the clear difference in the behavior of the two figures of merit R_S and X_S at different frequencies that can be observed in the time interval from 200 to 5500 s. This behavior can be used as an additional figure of merit to detect the presence of pollutant. It can be quantified for R_S as follows:

$$\text{max\_diff\_}R_S(t_n) = M_{R_S}(t_n) - m_{R_S}(t_n) \tag{3}$$

where, for each time instant t_n, $M_{R_S}(t_n)$ and $m_{R_S}(t_n)$ are the maximum and the minimum values of R_S measured over the seven considered frequencies, namely

$$M_{R_S}(t_n) = \max_f[R_S(t_n)] \text{ with } f \in \{1 \text{ kHz}|100 \text{ kHz}\} \tag{4}$$

$$m_{R_S}(t_n) = \min_f[R_S(t_n)] \text{ with } f \in \{1 \text{ kHz}|100 \text{ kHz}\}. \tag{5}$$

In the same manner, it can be defined the figure of merit that refers to X_S, say: max_diff_$X_S(t_n)$. The time evolution of such two figures of merit is reported in Fig. 11, for this experiment. They show a very similar behavior, being very close to zero in the absence of pollutant and increasing as the quantity of pollutant in the filter increases. Comparing these results to the issues discussed in the previous paragraph, we can conclude that the multifrequency approach solves the problem of the variation of the average value at the end. In addition, the cusps in Fig. 5 are no longer present.

The same approach has been used for test #2, with the double cycle of adsorption of acetonitrile, and the results are reported in Fig. 12. Also, in this case, it is possible to highlight the clear response of the considered figures of merit max_diff_R_S and max_diff_X_S: the two phases of pollutant "adsorption" and "evaporation" are clearly visible. It is also possible to notice that max_diff_X_S shows two identical cycles, whereas max_diff_R_S shows a lower peak value in the second cycle. This can be probably due to a residual presence of the pollutant in the interaction with the ring contacts that reduces the overall variation of the R_S parameter. We recall that, for this as well as for all the other experiments, the changes in the value of R_S or X_S in the absence of pollutant have been always compensated.

Finally, we summarize that the study of these two figures of merit, for the considered operating conditions, completes the information on the SoH of the filter, making evident not only both the absence and the presence of pollutant but also the

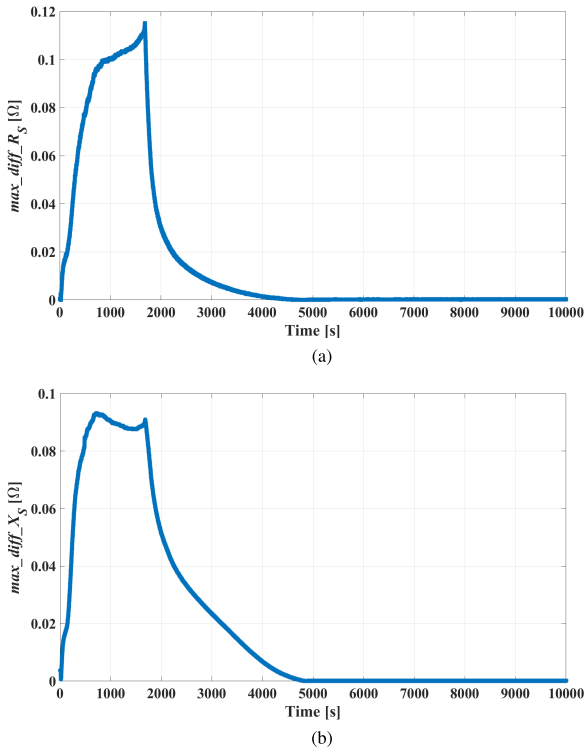

Fig. 11. Time behavior of the figures of merit: (a) max_diff_R_S and (b) max_diff_X_S, for test #1 (acetonitrile, multifrequency analysis from 1 to 100 kHz).

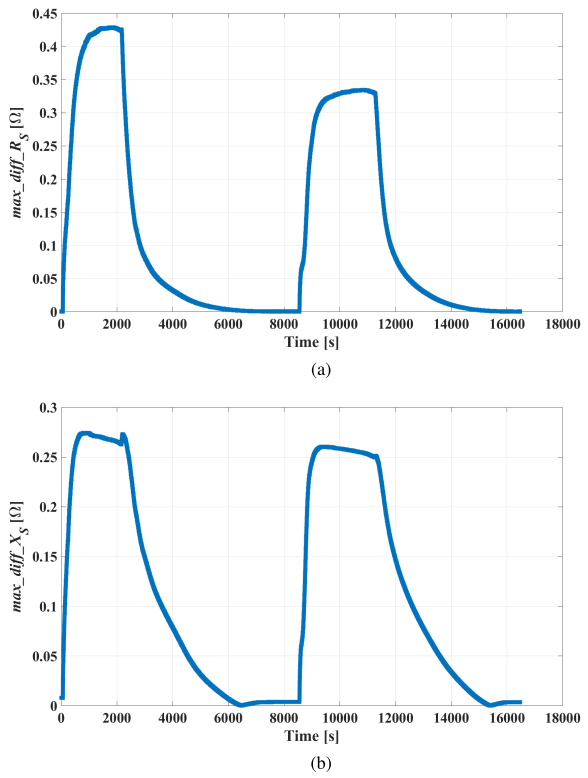

Fig. 12. Time behavior of the figures of merit: (a) max_diff_R_S and (b) max_diff_X_S, for test #2 (acetonitrile, double cycle, multifrequency analysis from 1 to 100 kHz).

aging state of the ring contact. In addition, by considering the volatility of the acetonitrile, these figures of merit give also

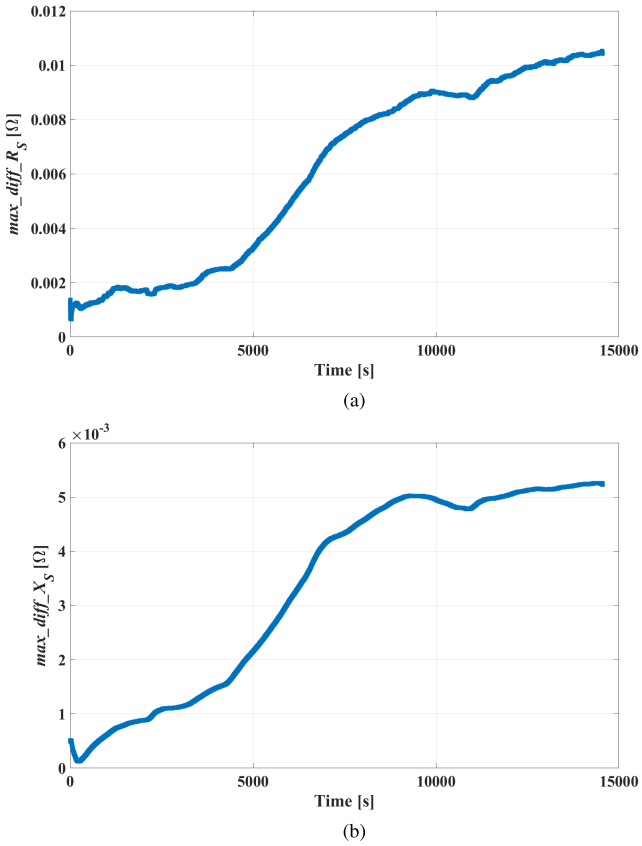

Fig. 13. Time behavior of the figures of merit: (a) max_diff_R_S and (b) max_diff_X_S, for test #3 (2,4-diclorophenol, multifrequency analysis from 1 to 100 kHz).

good indication about the evaporation of the pollutant from the filter.

The multifrequency approach has also been applied to the 2,4-dichlorophenol pollutant, e.g., test #3, whose results are reported in Fig. 13. In this case, it is possible to highlight [Fig. 13(a)] as this approach detrends the variation of R_S due to the interaction of the pollutant with the contact and highlights only the presence of the pollutant in the filter. This is a very important result since, for this kind of pollutant, it allows compensating the worsening of aging of the contact due to time or to the pollutant interaction. In addition, looking at Fig. 13, we can observe that both the figures of merit max_diff_R_S and max_diff_X_S clearly highlight the different phases of pollutant injections; this is evident from the changes in the slope that happen about every 2000 s. Finally, after the last injection of pollutant, at about the time equal to 10 000 s, a final increment is observed, and then, after 12000 s, a quite constant value is experimented.

A final analysis has been performed with test #4, with the single injection of 0.5 mL of 2,4-dichlorophenol, whose results are reported in Fig. 14. Also, in this case, the proposed figures of merit highlight the presence of the pollutant with a slope that is increased with respect to the previous test.

As a final remark, we note that a similar time behavior of the figures of merit observed for both pollutants may suggest a similar pollutant/filter interaction for the considered pollutants. A possible reason is that the adsorption is mediated

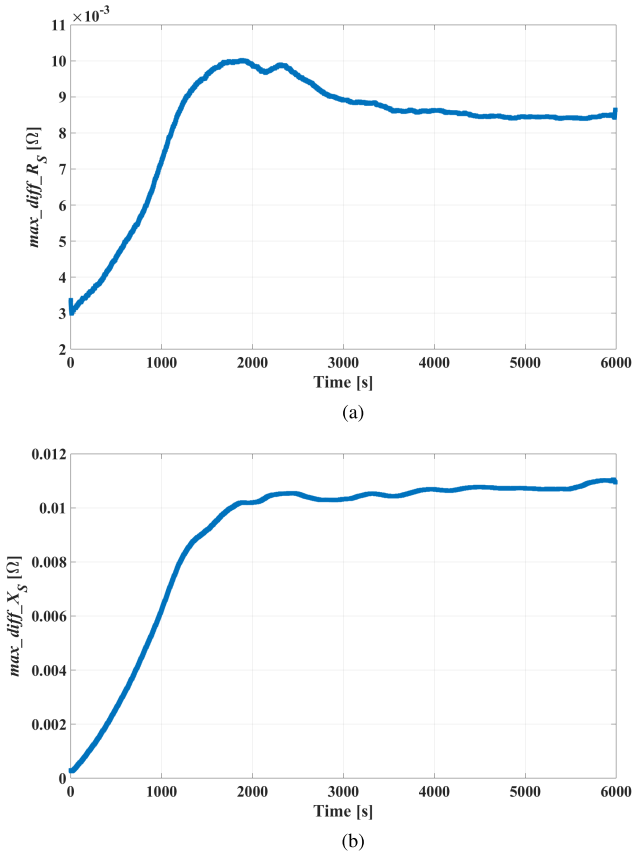

Fig. 14. Time behavior of the figures of merit: (a) max_diff_R_S and (b) max_diff_X_S, for test #4 (2,4-diclorophenol, multifrequency analysis from 1 to 100 kHz).

by Van der Waals interaction and mainly by $\pi-\pi$ interaction, due to the benzene ring in 2,4-dichlorophenol and to the triple bond in acetonitrile with aromatic system of GNP. In fact, the acetonitrile could interact with GNP in a parallel configuration, as recently demonstrated [34] and 2,4-dichlorophenol in stacking configuration, as well known from organic chemistry. Due to this consideration, the selectivity of pristine filters must be similar for both pollutants. Indeed, the estimation of the adsorption capability of the filter confirms this model: the quantity of molecules retained by filter is 17.6 $\pm$ 0.9 mmol/g for acetonitrile and 13 $\pm$ 1 mmol/g for 2,4-dichlorophenol. This small difference in this figure of merit will be investigated deeply in future research work; in fact, the difference could be attributed to the presence of a halogen atom on dichlorophenol or of a small porosity that entraps acetonitrile and excludes 2,4-dichlorophenol.

V. Conclusion

The real-time estimation of the LC of industrial filters through the measurement of the variation of their electrical impedance in the presence of pollutants is a novel solution that may open the way for novel predictive maintenance scenarios. Even though setups and methods related to this kind of measurement technique are cheap and simple, the reliability of the obtained results might worsen in the presence of nonidealities and uncertainties related to the aging of the contacts, the setup conditions, the interaction between the filter and the pollutant, and the changes in the environment. To overcome these problems, this article has proposed a novel monitoring technique based on the multifrequency excitation and the study of suitable figures of merit, which estimates the frequency-to-frequency distance of the real and imaginary parts of the measured impedance. This technique has been here applied to novel filters made by pressed graphene flakes (GNPs), exploiting the exceptional sensitivity of the electrical parameters of graphene materials when adsorbing external substances. Experiments carried out with acetonitrile and 2,4-dichlorophenol have confirmed the reliability of the proposed technique even in the presence of very different industrial pollutants. The demonstration of the proposed method encourages to make further steps in view of assessing a potential industrial application of this idea, which can be of interest for instance for enabling the predictive maintenance. With reference to the setup proposed here, an optimization step would be necessary, with reference to parameters that may strongly influence the performance, such as the GNP size or the GNP/electrode contact. In addition, other types of graphene-related materials may be investigated and compared to the GNPs adopted here, to check for instance the influence of the material-specific features such as the morphological characteristics (e.g., shape, aspect ratio, and roughness), the structural features (e.g., the defects' density), and/or the electrical parameters (e.g., frequency-dependent complex permittivity).

References

[1] S. Bonilla, H. Silva, M. Terra da Silva, R. Franco Gonçalves, and J. Sacomano, "Industry 4.0 and sustainability implications: A scenario-based analysis of the impacts and challenges," *Sustainability*, vol. 10, no. 10, p. 3740, Oct. 2018. [Online]. Available: https://www.mdpi.com/2071-1050/10/10/3740

[2] J. Yan, Y. Meng, L. Lu, and L. Li, "Industrial big data in an industry 4.0 environment: Challenges, schemes, and applications for predictive maintenance," *IEEE Access*, vol. 5, pp. 23484–23491, 2017.

[3] M. Compare, P. Baraldi, and E. Zio, "Challenges to IoT-enabled predictive maintenance for industry 4.0," *IEEE Internet Things J.*, vol. 7, no. 5, pp. 4585–4597, May 2020.

[4] D. A. C. Brownson and C. E. Banks, *The Handbook of Graphene Electrochemistry*. London, U.K.: Springer–Verlag, 2014.

[5] G. Cerro, M. Ferdinandi, L. Ferrigno, M. Laracca, and M. Molinara, "Metrological characterization of a novel microsensor platform for activated carbon filters monitoring," *IEEE Trans. Instrum. Meas.*, vol. 67, no. 10, pp. 2504–2515, Oct. 2018.

[6] Y. Wu, J. Zhu, and L. Huang, "A review of three-dimensional graphene-based materials: Synthesis and applications to energy conversion/storage and environment," *Carbon*, vol. 143, pp. 610–640, Mar. 2019. [Online]. Available: https://www.sciencedirect.com/science/article/pii/S0008622318310844

[7] H. Huang *et al.*, "Ultrafast viscous water flow through nanostrand-channelled graphene oxide membranes," *Nature Commun.*, vol. 4, no. 1, p. 2979, Dec. 2013.

[8] R. K. Joshi *et al.*, "Precise and ultrafast molecular sieving through graphene oxide membranes," *Science*, vol. 343, no. 6172, pp. 752–754, Feb. 2014. [Online]. Available: https://science.sciencemag.org/content/343/6172/752

[9] G. Zhao, J. Li, X. Ren, C. Chen, and X. Wang, "Few-layered graphene oxide nanosheets as superior sorbents for heavy metal ion pollution management," *Environ. Sci. Technol.*, vol. 45, no. 24, pp. 10454–10462, 2011. [Online]. Available: https://doi.org/10.1021/es203439v

[10] S. Vadahanambi, S.-H. Lee, W.-J. Kim, and I.-K. Oh, "Arsenic removal from contaminated water using three-dimensional graphene-carbon nanotube-iron oxide nanostructures," *Environmental Sci. Technol.*, vol. 47, no. 18, pp. 10510–10517, 2013. [Online]. Available: https://doi.org/10.1021/es401389g

[11] S. Y. Yang, C. D. Vecitis, and H. Park, "Electrocatalytic water treatment using carbon nanotube filters modified with metal oxides," *Environ. Sci. Pollut. Res.*, vol. 26, no. 2, pp. 1036–1043, Jan. 2019.

[12] Z. Sui, Q. Meng, X. Zhang, R. Ma, and B. Cao, "Green synthesis of carbon nanotube–graphene hybrid aerogels and their use as versatile agents for water purification," *J. Mater. Chem.*, vol. 22, no. 18, pp. 8767–8771, 2012, doi: 10.1039/C2JM00055E.

[13] F. Cecen and O. Aktas, *Activated Carbon for Water and Wastewater Treatment: Integration of Adsorption and Biological Treatment*. Weinheim, Germany: Wiley-VCH Verlag GmbH & Co. KGaA, 2011.

[14] R. J. Young, I. A. Kinloch, L. Gong, and K. S. Novoselov, "The mechanics of graphene nanocomposites: A review," *Composites Sci. Technol.*, vol. 72, no. 12, pp. 1459–1476, Jul. 2012. [Online]. Available: https://www.sciencedirect.com/science/article/pii/S0266353812001789

[15] A. Dabrowska, S. Bellucci, A. Cataldo, F. Micciulla, and A. Huczko, "Nanocomposites of epoxy resin with graphene nanoplates and exfoliated graphite: Synthesis and electrical properties," *Phys. Status Solidi B*, vol. 251, no. 12, pp. 2599–2602, Dec. 2014. [Online]. Available: https://onlinelibrary.wiley.com/doi/abs/10.1002/pssb.201451175

[16] M. Potenza, A. Cataldo, G. Bovesecchi, S. Corasaniti, P. Coppa, and S. Bellucci, "Graphene nanoplatelets: Thermal diffusivity and thermal conductivity by the flash method," *AIP Adv.*, vol. 7, no. 7, Jul. 2017, Art. no. 075214, doi: 10.1063/1.4995513.

[17] M. Molinara, M. Ferdinandi, G. Cerro, L. Ferrigno, and E. Massera, "An end to end indoor air monitoring system based on machine learning and SENSIPLUS platform," *IEEE Access*, vol. 8, pp. 72204–72215, 2020.

[18] L. Ferrigno, A. Cataldo, S. Sibilia, A. Maffucci, and S. Bellucci, "A monitorable and renewable pollution filter based on graphene nanoplatelets," *Nanotechnology*, vol. 31, no. 7, Nov. 2019, Art. no. 075701, doi: 10.1088/1361-6528/ab5072.

[19] L. Ferrigno, M. Laracca, C. Liguori, and A. Pietrosanto, "An FPGA-based instrument for the estimation of R , L, and C parameters under nonsinusoidal conditions," *IEEE Trans. Instrum. Meas.*, vol. 61, no. 5, pp. 1503–1511, Dec. 2012.

[20] L. Ferrigno, M. Laracca, and A. Pietrosanto, "Measurement of passive R, L, and C components under nonsinusoidal conditions: The solution of some case studies," *IEEE Trans. Instrum. Meas.*, vol. 57, no. 11, pp. 2513–2521, May 2008.

[21] L. Ferrigno, C. Liguori, and A. Pietrosanto, "Measurements for the characterization of passive components in non-sinusoidal conditions," *IEEE Trans. Instrum. Meas.*, vol. 51, no. 6, pp. 1252–1258, Dec. 2002.

[22] L. Ferrigno, A. Maffucci, G. Miele, S. Sibilia, S. Bellucci, and A. Cataldo, "Multi-frequency signal for saturation detection of a pollution filter based on graphene nanoplatelets," in *Proc. IEEE Int. Instrum. Meas. Technol. Conf. (I MTC)*, May 2020, pp. 1–6.

[23] P. Wexler, *Encyclopedia of Toxicology*, 2nd ed. Oxford, U.K.: Elsevier, 2005.

[24] J. J. Freeman and E. P. Hayes, "Microsomal metabolism of acetonitrile to cyanide: Effects of acetone and other compounds," *Biochem. Pharmacol.*, vol. 37, no. 6, pp. 1153–1159, Mar. 1988, doi: 10.1016/0006-2952(88)90524-2

[25] Y.-Y. Chao, Y.-M. Tu, Z.-X. Jian, H.-W. Wang, and Y.-L. Huang, "Direct determination of chlorophenols in water samples through ultrasound-assisted hollow fiber liquid–liquid–liquid microextraction on-line coupled with high-performance liquid chromatography," *J. Chromatography A*, vol. 1271, no. 1, pp. 41–49, Jan. 2013. [Online]. Available: https://www.sciencedirect.com/science/article/pii/S0021967312017724

[26] S. C. Smith and D. F. Rodrigues, "Carbon-based nanomaterials for removal of chemical and biological contaminants from water: A review of mechanisms and applications," *Carbon*, vol. 91, pp. 122–143, Sep. 2015. [Online]. Available: https://www.sciencedirect.com/science/article/pii/S0008622315003346

[27] G. Crini and P.-M. Badot, "Application of chitosan, a natural aminopolysaccharide, for dye removal from aqueous solutions by adsorption processes using batch studies: A review of recent literature," *Prog. Polym. Sci.*, vol. 33, no. 4, pp. 399–447, Apr. 2008. [Online]. Available: https://www.sciencedirect.com/science/article/pii/S0079670007001293

[28] T. Hüffer, S. Endo, F. Metzelder, S. Schroth, and T. C. Schmidt, "Prediction of sorption of aromatic and aliphatic organic compounds by carbon nanotubes using poly-parameter linear free-energy relationships," *Water Res.*, vol. 59, pp. 295–303, Aug. 2014. [Online]. Available: https://www.sciencedirect.com/science/article/pii/S0043135414003145

[29] Y. Shunin, S. Bellucci, A. Gruodis, and T. Lobanova-Shunina, *Non-regular Nanosystems–Theory and Applications*. Cham, Switzerland: Springer, 2018.

[30] Y. Shunin *et al.*, "Nanosensor devices for CBRN-agents detection: Theory and design," in *Nanostructured Materials for the Detection of CBRN*, J. Bonča and S. Kruchinin, Eds. Dordrecht, The Netherlands: Springer, 2018, pp. 169–184.

[31] A. Zubiarrain-Laserna and P. Kruse, "Review graphene-based water quality sensors," *J. Electrochem. Soc.*, vol. 167, no. 3, Jan. 2020, Art. no. 037539, doi: 10.1149/1945-7111/ab67a5.

[32] S. Bellucci, "Development of biosensors using carbon nanotubes and few layered graphene," in *Nanostructured Materials for the Detection of CBRN*, J. Bonča and S. Kruchinin, Eds. Dordrecht, The Netherlands: Springer, 2018, pp. 19–29.

[33] S. Bellucci, A. Cataldo, L. Ferrigno, S. Giovannetti, and A. Maffucci, "An impedance-based life-monitoring technique for a graphene water filter," in *ELECTRIMACS 2019*, W. Zamboni and G. Petrone, Eds. Cham, Switzerland: Springer, 2020, pp. 719–726.

[34] M. Tylinski, R. S. Smith, and B. D. Kay, "Structure and desorption kinetics of acetonitrile thin films on Pt(111) and on graphene on Pt(111)," *J. Phys. Chem. C*, vol. 124, no. 4, pp. 2521–2530, Jan. 2020, doi: 10.1021/acs.jpcc.9b10579.

Gianfranco Miele (Senior Member, IEEE) received the M.S. degree *(cum laude)* in telecommunication engineering and the Ph.D. degree in electrical and information engineering from the University of Cassino, Cassino, Italy, in 2004 and 2008, respectively.

Since 2019, he has been an Associate Professor with the Department of Electrical and Information Engineering, University of Cassino and Southern Lazio, Cassino. He has authored or coauthored about 70 journal articles and conference papers in instrumentation and measurements. His current research interests include electrical and electronic measurements, in particular, the design and implementation of innovative methods for performance assessment of RF telecommunication systems and communication networks, image-based measurement systems, measurement of electromagnetic compatibility, and DSP-based measurement systems.

Dr. Miele is a member of the Italian Association "Electrical and Electronic Measurements Group," the IEEE Instrumentation and Measurement Society, and IEEE 802.22 and IEEE 802.15 Working Groups. In 2008, he was a recipient of the Carlo Offelli Prize for the best Ph.D. dissertation in electronic measurement.

Stefano Bellucci received the Laurea degree *(summa cum laude)* in physics from the Sapienza University of Rome, Rome, Italy, in 1982, and the Ph.D. degree in physics of elementary particles from the International School for Advanced Studies (SISSA), Trieste, Italy, in 1986.

He worked as a Research Associate at Brandeis University, Waltham, MA, USA, from 1983 to 1985; and a Visiting Researcher at the Massachusetts Institute of Technology, Cambridge, MA, USA, from 1985 to 1986, the University of Maryland, College Park, MD, USA, from 1986 to 1987, and the University of California at Davis, Davis, CA, USA, from 1987 to 1988. He was appointed as a Tenured Researcher (Research Staff) at the Istituto Nazionale di Fisica Nucleare–Laboratori Nazionali di Frascati (INFN-LNF) in 1987. He was appointed as an INFN First Researcher (Senior Research Staff) in 2005. Italy Ministry of University in 2013 habilitated him as a Full Professor in Theoretical Physics of Fundamental Interactions and in Theoretical Condensed Matter Physics. He is also the Director of the NATO Emerging Security Challenges Division, SPS Program projects "Nanocomposite based photonic crystal sensors of biological and chemical agents." He is the Principal Investigator of the Time2Quest Condensed Matter Theory INFN CSN4 project and Research Group Projects 2020 "High Pressure Sanification of Water for Foodborne Virus removal (HPSWFood)." He is an INFN scientist in charge of the Ministry for University and Research project "a Smart Framework for vIrus Detection (SFIDE)." He coordinated all LNF theoretical physics activities from 1999 to 2002 and 2011 to 2015. He has published 600 articles

with 14 016 citations (4717 citations since 2016) in peer-reviewed journals with Hirsch index h = 55 and 20 invited book chapters. He is an editor and/or a coauthor of over ten books with Springer. His research interests include theoretical physics, condensed matter, biophysics, physical chemistry, nanoscience and nanotechnology, nanocarbon-based composites, toxicology, and biomedical applications.

Dr. Bellucci received the B.W. Lee Prize at the Erice School of Subnuclear Physics, Erice, Italy, in 1982. He was in the list of Top Italian Scientists published by the VIA Academy. In 1980, he was selected as a Summer Student at CERN, Geneva, Switzerland. He is the Editor-in-Chief of the Section Carbon *Materials* (MDPI), a Series Editor of *Lecture Notes in Nanoscale Science and Technology* (Springer), and an Associate Editor of *Hindawi Journal of Nanomaterials*. His lab cultivated over 40 Ph.D. and master students.

Antonino Cataldo received the master's degree *(cum laude)* in chemistry (with a specialization in physical chemistry) and the Ph.D. degree in chemistry, with a focus on structural and functional properties of nanocomposites from the University of Palermo, Palermo, Italy, in 2011 and 2015, respectively.

During the Ph.D. degree, he worked as a Research Fellow at the Istituto Nazionale di Fisica Nucleare–Laboratori Nazionali di Frascati (INFN-LNF), in the nanotechnology group NEXT, (Prof. S. Bellucci). He was a Research Fellow at University of Chieti Pescara, Chieti, Italy, from 2016 to 2018, and INFN-LNF from 2018 to 2019. Up to 2021, he was a Research Fellow at the Department of Information Engineering (DII), Polytechnic University of Marche, Ancona, Italy, where he was involved in the UE project "Artificial permittivity and permeability engineering for future generation subwavelength analog integrated circuits and systems"—NANOPOLY. In particular, he develops new simulation methods for components based on metamaterial and nanomaterial, and characterization on metamaterials and 2-D materials. He is currently a Researcher at the Technologies Laboratory for Structural Dynamics, ENEA Casaccia Research Center, Rome, Italy, where he is involved in the prevention of seismic and hydrogeological risk (DISPREV). He has 755 citations (H-index: 15) and more than 40 articles in international peer-reviewed journals.

Alessio Di Tinno received the M.S. degree *(cum laude)* in chemical science and technologies from the Department of Analytical Chemistry, University of Rome "Tor Vergata," Rome, Italy, in December 2019.

Mr. Di Tinno has been awarded as best student of the course of Applied Chemistry in 2017, 5% of University best students in 2018, and best Master Degree Thesis in Chemistry in 2019. In 2020, he received a post-graduate scholarship of 12 months at the Department of Electrical and Information Engineering, University of Cassino and Southern Lazio, Cassino, Italy, where he had the opportunity to work on the development of electrochemical sensors and biosensors applied in the determination of organic and inorganic pollutants.

Luigi Ferrigno (Senior Member, IEEE) has been a Full Professor of electric and electronic measurement and the Scientific Manager of the Industrial Measurements Laboratory, University of Cassino, Cassino, Italy, since 2004. In 2008, he was a Founding Member of the university spin-off, Spring Off (University of Salerno), Fisciano, Italy. He is an NDE4.0 Ambassador for the Italian Association of Non-Destructive Evaluation and Test (AiPnD) in the EFNDT WG10. He coordinated and participated in several national and international research projects. His current research interests include the NDT4.0, novel learning sensors and measurement systems for smart city, the Internet of Things (IoT), automotive, smart energy, and environment.

Antonio Maffucci (Senior Member, IEEE) received the Laurea degree *(summa cum laude)* in electronic engineering and the Ph.D. degree in electrical engineering from the University of Naples Federico II, Italy, in 1996 and 2000, respectively.

In 1997, he was with the Nuclear Fusion Laboratory JET, Culham, U.K. From 1998 to 2002, he was with the Department of Electrical Engineering, University of Naples Federico II. He is currently a Full Professor of electrotechnics with the Department of Electrical and Information Engineering, University of Cassino and Southern Lazio, Cassino, Italy, and a Research Associate at the National Institute of Nuclear Physics, Istituto Nazionale di Fisica Nucleare–Laboratori Nazionali di Frascati (INFN-LNF), Frascati, Italy. He is the Coordinator of the EU-H2020 project "TERASSE" and the NATO-SPS project "2DSENSE." He is the author of about 200 technical articles on international journals, conference proceedings, and essays on books. He has coauthored the books *Transmission Lines and Lumped Circuits* (Academic Press, 2001), *Fundamentals of Applied Nanoelectromagnetics* (Springer, 2016 and 2019), *Carbon Nanotube for Interconnects* (Springer, 2016), and *Carbon-Based Nano-Electromagnetics* (Elsevier, 2019). His research areas include computational electromagnetics, electromagnetic compatibility, distributed circuit and systems, nanoelectronics, and quantum circuits.

Dr. Maffucci is a member of the IEEE Nanopackaging Council, the Editorial Boards of *Applied Sciences*, and *Journal of Nanoscience and Nanotechnology Applications*. He is also a member of several committees of international conferences. He was the General Chairman of the conferences IEEE SPI 2011 and 2012 and the workshops FANEM 2015 and 2018. He serves as an Associate Editor for the IEEE TRANSACTIONS ON COMPONENTS, PACKAGING, AND MANUFACTURING TECHNOLOGY.

Laura Micheli is currently an Associate Professor at the University of Rome, Rome, Italy, and she has strong background on immunoassays for clinical and environmental analysis. She has been involved in the development of traditional and label-free immunosensors and biosensors based on screen-printed electrodes (SPE) in the fields of environmental, clinical, and food analysis. She has published about 66 articles in international journals (H-Index Scopus: 23). Her research activity is focused on the study and development of "disposable" electrochemical tools for the determination of different analytes in food, the clinical and food field, and the field of cultural heritage using spectrophotometric and chromatographic methods for their validation.

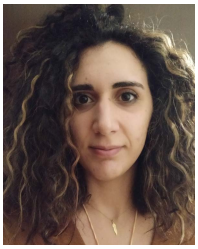

Sarah Sibilia received the B.Sc. and M.Sc. degrees in electrical engineering from the University of Cassino and Southern Lazio, Cassino, Italy, in 2016 and 2019, respectively.

Since 2019, she has been a Research Fellow with the Department of Electrical and Information Engineering, University of Cassino and Southern Lazio. She is involved in international and national research projects on these topics: "TERASSE" (EU-H2020), "2DSENSE" (NATO-SPS), and "AIRETEC" (Region LAZIO). Her main research interests include electric, electrothermal, and electromagnetic modeling and experimental characterization of nanomaterials and nanotechnological devices.